The Nonlinear Interaction of Barotropic and Equatorial Baroclinic Rossby Waves

ANDREW J. MAJDA

Courant Institute of Mathematical Sciences, Center for Atmosphere–Ocean Science, New York University, New York, New York

JOSEPH A. BIELLO

Department of Mathematical Sciences, Rensselaer Polytechnic Institute, Troy, New York

(Manuscript received 12 September 2002, in final form 12 February 2003)

ABSTRACT

Simplified asymptotic equations are developed for the nonlinear interaction of long-wavelength equatorial Rossby waves and barotropic Rossby waves with a significant midlatitude projection in the presence of suitable horizontally and vertically sheared zonal mean flows. The simplified equations allow for nonlinear energy exchange between the barotropic Rossby waves and the baroclinic equatorial waves for nonzero zonal mean vertical shear through wave–wave interactions. Idealized examples in the model demonstrate that midlatitude Rossby wave trains in a baroclinic mean shear can transfer their energy to localized equatorially trapped baroclinic Rossby waves through a nonlinear ''westerly wind burst'' mechanism. Conversely, equatorially trapped baroclinic Rossby wave trains in the idealized model can transfer substantial energy to the midlatitude barotropic Rossby waves. From the viewpoint of applied mathematics, the asymptotic equations derived here have several novel features.

1. Introduction

The lateral exchange of energy in the troposphere between the midlatitudes and the equatorial region is a topic of considerable significance for understanding global teleconnection patterns from the Tropics to the midlatitudes as well as the midlatitude influence on tropical wave dynamics in monsoons, the Madden–Julian intraseasonal oscillation, and El Niño. Since a significant portion of the energy in the atmosphere is in equivalent barotropic modes, an important theoretical issue is the exchange of energy in the troposphere between equatorially trapped waves and equivalent barotropic modes with a significant projection on midlatitude dynamics. To gain basic insight into the fashion in which tropical heating yields a midlatitude response, Webster (1972, 1981, 1982) utilized a linearized two-layer global primitive equation model to show that localized steady tropical forcing can have a significant midlatitude barotropic response for a zonal mean climatology with both horizontal and vertical shear. Kasahara and Silva Dias (1986) did analogous studies with a linearized global primitive equation model and confirmed the earlier conclusion of Webster that vertical and horizontal mean shear are needed in order to generate a significant midlatitude response, which is largely equivalent barotropic. Hoskins and Jin (1991) did a similar linearized study with the primitive equations for the transient response to localized tropical forcing and confirmed the importance of mean shear in the horizontal and vertical in generating a significant midlatitude response; this work showed the importance of nearly dispersionless long-wavelength equatorial Rossby waves in generating the midlatitude response. To gain theoretical insight into these issues, Wang and Xie (1996) performed a linear stability analysis for an equatorial β-plane two-layer model around basic zonal states with horizontal and vertical shear; their results showed that at large scales, $m = 1$, equatorial Rossby waves (ER) strongly coupled to barotropic waves in the midlatitudes as linearized characteristic modes of propagation provided that there is vertical shear in the zonal background state; furthermore, the dispersion relation of the long-wavelength, $m = 1$, ER waves at large scales is modified significantly by the presence of a mean vertical shear. As regards the forcing of the Tropics by midlatitude waves, Lim and Chang (1981, 1986) have suggested the importance of vertical mean shear for a significant response while Hoskins and Yang (2000) have emphasized the role of nearly resonant forcing in several specific physical mechanisms. Recently Lin et al. (2000) showed the significance of midlatitude dynamics in triggering tropical intraseasonal responses in an intermediate climate model with essentially two vertical modes of resolution: a barotropic mode and a baroclinic heating mode.

Corresponding author address: Prof. Andrew J. Majda, Courant Institute of Mathematical Sciences, New York University, 251 Mercer Street, New York, NY 10012.
E-mail: jonjon@cims.nyu.edu

All of the work cited earlier suggests a fundamental theoretical issue: How do large-scale transient barotropic waves with a significant midlatitude projection and large-scale equatorial baroclinic waves exchange energy nonlinearly in the presence of mean shear? The objective of the present study is to answer these two basic questions in an idealized setting. Motivated by the work of Webster (1972, 1981, 1982) and Wang and Xie (1996) the basic nonlinear dynamic equations utilized here are the two-layer equatorial β-plane equations rescaled at long zonal wavelengths; these equations allow for both barotropic and equatorial baroclinic waves and are presented briefly in section 2. Resonant interactions between nearly dispersionless long-wavelength equatorial Rossby waves and barotropic Rossby waves with a significant midlatitude projection are identified through linear theory in section 3. Studying such nearly dispersionless long-wavelength waves is suggested by the work of Hoskins and Jin (1991) as discussed earlier. Then, a suitable weakly nonlinear asymptotic expansion is utilized to derive simplified dynamic equations for the nonlinear interaction of such near-resonant long-wavelength barotropic wave trains and equatorial baroclinic wave trains with a zonal shear. The basic properties of the reduced asymptotic model are studied in section 4 including barotropic–baroclinic energy budgets and a simple linearized stability analysis around suitable meridionally and vertically sheared basic states. The linear stability results for the asymptotic model are transparent yet analogous to those of Wang and Xie (1996). In section 5 the basic questions of nonlinear midlatitude–tropical energy transfer are addressed in the simplified asymptotic model. The nonlinear asymptotic model equations developed in this paper are novel equations in the applied mathematics literature in many aspects. These facts as well as potential further applications of the present theory with dissipation and forcing are discussed briefly in the summary in section 6.

2. The two-layer equatorial β-plane equations

In standard nondimensional units defined later, the two-layer equatorial β-plane equations for the barotropic and baroclinic horizontal velocity and pressure, $\mathbf{v}_0$, p_0, and $\mathbf{v}_1$, p_1, respectively, are given by

$$\frac{\overline{D}}{Dt}\mathbf{v}_0 + y v_0^{\perp} + \mathbf{v}_1 \,\mathrm{div}(\mathbf{v}_1) + (\mathbf{v}_1 \cdot \nabla)\mathbf{v}_1 = -\nabla p_0$$

$$\mathrm{div}\mathbf{v}_0 = 0 \qquad (2.1)$$

$$\frac{\overline{D}}{Dt}\mathbf{v}_1 + y v_1^{\perp} + (\mathbf{v}_1 \cdot \nabla)\mathbf{v}_0 = -\nabla p_1$$

$$\frac{\overline{D}}{dt}p_1 + \mathrm{div}\mathbf{v}_1 = 0. \qquad (2.2)$$

In (2.1) and (2.2) $\mathbf{v}_j = (u_j, v_j)$, $\mathbf{v}_j^{\perp} = (-v_j, u_j)$, p_j for $j = 1, 2$ are functions of the horizontal variable, (x, y) alone and all the vector derivatives involve only horizontal differentiation. Here and elsewhere in the paper the transport operator, $\overline{D}/Dt = \partial/\partial t + \mathbf{v}_0 \cdot \nabla$. represents advection by the barotropic mode. The nonlinear equations for the interaction of barotropic and baroclinic modes in (2.1), (2.2) can be derived in standard fashion (Neelin and Zeng 2000; Majda and Shefter 2001) from a two-vertical-mode Galerkin truncation of the Boussinesq equations with rigid-lid boundary conditions with the form

$$\mathbf{v} = \mathbf{v}_0 + \mathbf{v}_1\sqrt{2}\,\cos\left(\frac{\pi z}{H}\right)$$

$$p = p_0 + p_1\sqrt{2}\,\cos\left(\frac{\pi z}{H}\right), \qquad (2.3)$$

where $c = H\overline{N}/\pi$ is the corresponding gravity wave speed determined by the Brunt–Väisälä frequency, $\overline{N} = 10^{-2}\ \mathrm{s}^{-1}$, and the equivalent depth, H. In (2.1) and (2.2) the equations have been nondimensionalized through the units of length measured by the equatorial Rossby radius, $L_E = (c/\beta)^{1/2}$ and time given by $T_E = (c\beta)^{-1/2}$ while velocity and pressure are nondimensionalized by c and c^2, respectively. Later, the standard values associated with dry wave propagation of a baroclinic heating mode with

$$c = 50\ \mathrm{m\ s}^{-1}, \quad T_E = 8.3\ \mathrm{hr}, \quad L_E = 1500\ \mathrm{km} \qquad (2.4)$$

are utilized to demonstrate various qualitative effects of the nonlinear coupling in (2.1), (2.2).

An alternative derivation of the linearized version of these equations can be found in Wang and Xie (1996). Here the β-plane approximation centered at the equator is utilized for barotropic Rossby waves, which extend meridionally to 3.6 L_E, approximately 50° north and south. These values are at the margin of the β-plane approximation compared with full-spherical geometry; at least for the linear theory studied here in section 4, Wang and Xie (1996) have shown that the β-plane approximation is quite accurate for the issues considered here even for this rather large meridional extent.

Note that as for the primitive equations, the total energy of both barotropic and baroclinic modes,

$$E = \frac{1}{2}\int |\mathbf{v}_0|^2 + \frac{1}{2}\int |\mathbf{v}_1|^2 + |p_1|^2 = E_{\mathrm{BT}} + E_{\mathrm{BC}}, \qquad (2.5)$$

is conserved by (2.1) and (2.2).

With the streamfunction, ψ, satisfying $u_0 = -\psi_y$, $v_0 = \psi_x$, the barotropic equations in (2.1) are reduced to an equivalent scalar equation for ψ by taking the curl of the first equation in (2.1). The result is the equation

$$\frac{\overline{D}}{Dt}\Delta\psi + \psi_x + \mathrm{div}[-(\mathbf{v}_1 u_1)_y + (\mathbf{v}_1 v_1)_x] = 0. \qquad (2.6)$$

While forcing effects for (2.1) and (2.2) due to tropical

heating, radiative damping, and boundary layer drag are all important for generating the transient dynamics, the emphasis here is on the nonlinear exchange of energy between transient large-scale barotropic and equatorial baroclinic wave trains through nonlinear advection alone. Thus, such forcing effects are omitted here for simplicity in exposition. Also, with rigid-lid boundary conditions at the top of the troposphere, potential additional dissipation through radiation of waves in the stratosphere is not considered here.

The zonal long-wave scaling

In the zonal long-wave scaling for the coupled equations in (2.2) and (2.6), zonal variations in x are assumed to occur on the longer basic length scale, L, with corresponding weaker meridional velocities and a longer basic unit of time, T, satisfying

$$\frac{L_E}{L} = \delta, \qquad \frac{T_E}{T} = \delta, \qquad |v| = \delta|u|, \tag{2.7}$$

for $\delta \ll 1$. Assume that the solutions of interest for (2.2) and (2.6) vary on scales compatible with (2.7); thus, in the original nondimensional units, assume

$$\psi = \psi(\delta x, y, \delta t), \qquad p_1 = p_1(\delta x, y, \delta t)$$
$$u_1 = u_1(\delta x, y, \delta t), \qquad v_1 = \delta v_1(\delta x, y, \delta t). \tag{2.8}$$

For solutions with the special form (2.8), the equations in (2.2) and (2.6) become the Long-Wave-Scaled Equatorial Baroclinic–Barotropic Equations (LWSEBB)

$$\frac{\overline{D}}{Dt}u_1 - \mathbf{v}_1 \cdot \nabla\psi_y - yv_1 + (p_1)_x = 0$$
$$\frac{\overline{D}}{Dt}p_1 + \mathrm{div}(\mathbf{v}_1) = 0$$
$$(p_1)_y + yu_1 + \delta^2\left(\frac{\overline{D}}{Dt}v_1 + \mathbf{v}_1 \cdot \nabla\psi_x\right) = 0 \quad \text{and} \tag{2.9}$$
$$\frac{\overline{D}}{Dt}(\psi_{yy}) + \psi_x - \mathrm{div}[(\mathbf{v}_1 u_1)_y] + \delta^2\left\{\frac{\overline{D}}{Dt}(\psi_{xx}) + \mathrm{div}[(\mathbf{v}_1 v_1)_x]\right\} = 0. \tag{2.10}$$

To avoid cumbersome notation, the arguments of the variables displayed in (2.8) are written implicitly in (2.9) and (2.10) and are still denoted by x, y, t in section 3.

3. Asymptotic equations for the interaction of barotropic and equatorial baroclinic waves

Here the reduced asymptotic equations are derived systematically. First, note that to leading order in δ, the LWSEBB equations in (2.9) and (2.10) linearized about a zero background state reduce to the decoupled linear equatorial long-wave equation (Heckley and Gill 1984) and the linear barotropic long-wave equations, respectively. The linear barotropic long-wave equation has the familiar dispersion relation, $\omega_B = -(k/l^2)$, with corresponding dispersionless Rossby wave train solutions,

$$\psi = -B(x - c_{\mathrm{BT}}t)\sin(ly), \qquad c_{\mathrm{BT}} = -\frac{1}{l^2} \tag{3.1}$$

for any wavenumber l. Similarly, the linear equatorial long-wave equation has dispersionless equatorial Rossby wave train solutions (Heckley and Gill 1984)

$$\begin{pmatrix} p \\ u \\ v \end{pmatrix} = \begin{Bmatrix} -\dfrac{A_m(x - c_m t)}{\sqrt{2}}\left[D_{m-1} + \dfrac{D_{m+1}}{(m+1)}\right] \\ \dfrac{A_m(x - c_m t)}{\sqrt{2}}\left[D_{m-1} - \dfrac{D_{m+1}}{(m+1)}\right] \\ -\left(\dfrac{2}{2m+1}\right)\dfrac{\partial A_m(x - c_m t)}{\partial x}D_m \end{Bmatrix} \tag{3.2}$$

for any integer $m > 0$, where $D_k(y)$ are the parabolic cylinder functions. Here and throughout the paper, m is used for the meridional index of the equatorial wave and n is used to index zonal wavenumbers. For a fixed m, the dispersionless packets in (3.1) and (3.2) are resonant for a meridional wavelength, L_* with $l = (2\pi/L_*)L_E$ for the barotropic mode provided that

$$c_{\mathrm{BT}}(L_*) = c_m, \qquad l = \sqrt{2m+1}, \quad \text{or}$$
$$L_* = -\frac{2\pi}{\sqrt{2m+1}}L_E \tag{3.3}$$

for $m = 1, 2, 3, \ldots$ Note that the equatorial Kelvin wave is never nearly resonant with a barotropic Rossby wave. With the gravity wave speed, $c = 50$ m s^{-1} and $L_E = 1500$ km from (2.4), the dimensional meridional wavelengths of the resonant barotropic Rossby waves are approximately

$$L_* \cong 3.6L_E = 5440 \text{ km} \quad \text{for } m = 1$$
$$L_* \cong 2.8L_E = 4200 \text{ km} \quad \text{for } m = 2$$
$$L_* \cong 2.4L_E = 3600 \text{ km} \quad \text{for } m = 3 \tag{3.4}$$

so that the barotropic Rossby wave trains have a substantial midlatitude projection for $m = 1, 2$. The $m = 3$ equatorial Rossby wave is less concentrated near the equator and already has a significant midlatitude projection so it will not be emphasized here. Next, reduced asymptotic equations are derived for the nonlinear interaction of such nearly resonant equatorial Rossby and barotropic wave trains with a mean zonal shear flow.

a. The reduced asymptotic model

Motivated by (3.1), (3.2), and (3.3), here small-amplitude weakly nonlinear solutions of the LWSEBB equations (2.9) and (2.10) are constructed with the form,

$$\psi = -\epsilon B(x - c_m t, \epsilon t)\sin(ly) + \epsilon^2\psi_2(x, y, t, \epsilon t)$$

$$p_{\rm BC} = -\epsilon\frac{A(x - c_m t, \epsilon t)}{\sqrt{2}}\left[D_{m-1} + \frac{D_{m+1}}{(m+1)}\right] + \epsilon^2 p_2(x, y, t, \epsilon t)$$

$$u_{\rm BC} = \epsilon\frac{A(x - c_m t, \epsilon t)}{\sqrt{2}}\left[D_{m-1} - \frac{D_{m+1}}{(m+1)}\right] + \epsilon^2 u_2(x, y, t, \epsilon t)$$

$$v_{\rm BC} = -\epsilon\left(\frac{2}{2m+1}\right)\frac{\partial A(x - c_m t, \epsilon t)}{\partial x}D_m + \epsilon^2 v_2(x, y, t, \epsilon t), \quad (3.5)$$

where l and c_m satisfy the resonance condition in (3.3). In order to have weak dispersive effects compete with nonlinearity in these long-wave solutions (Boyd 1980; Pantoine and Warn 1982), the zonal long-wave parameter δ in (2.9) and (2.10) and the amplitude, ϵ, in (3.5) are balanced and satisfy $\delta^2 = \epsilon$. As discussed in detail in section 4b, the reasonable value of $\epsilon = 0.1$ allows zonal velocities of order 5 m s^{-1} and with $\delta^2 = \epsilon$, zonal variation on scales of order 5000 km; thus the relation $\delta^2 = \epsilon$ is physically realistic.

As shown later, solvability conditions to second order in ϵ for the expansion in (3.5) with this relationship of δ to ϵ yield the following Reduced Equations for Equatorial Baroclinic–Barotropic Waves (REEBBW):

$$r_A A_\tau - D_A A_{xxx} + \alpha B A_x + \beta A B_x = 0$$

$$r_B B_\tau - D_B B_{xxx} + \gamma A A_x = 0, \quad (3.6)$$

the coefficients r_A, r_B, D_A, D_B, α, β, γ being given explicitly later in (3.10) with r_A, $r_B > 0$. In (3.6), $\tau = \epsilon t$ is the long time variable while $A_\tau = \partial A/\partial\tau$ etc. The explicit coefficients α, β, γ in (3.6) listed below in (3.10) and (3.12) satisfy $\alpha - 2\beta + \gamma = 0$ so that the reduced equations conserve the total energy

$$E = \frac{1}{2}\int r_B B^2 + \frac{1}{2}\int r_A A^2 = E_{\rm BT} + E_{\rm BC}. \quad (3.7)$$

This property reflects the energy conservation principle in (2.5). Recall from the earlier discussion (2.4) that zonal velocities are nondimensionalized by c in (2.9), (2.10) so that for $c = 50$ m s^{-1} and the conservative small-amplitude value, $\epsilon = 0.1$ in the asymptotics, reasonable dimensional barotropic and baroclinic velocities of order 5 m s^{-1} are allowed in the nonlinear dynamics in (3.6). More detailed discussion of such dimensional values is presented later for interpreting the solutions of (3.6) in a physical setting. With (2.8), the zonal averages, $\overline{A}(\tau) \equiv \int A(x, \tau)\,dx$ and $\overline{B}$ give vertical and horizontal zonal shear components, which project strongly on the equatorial jet and trade winds regimes for $m = 1$; this is shown in Fig. 1 where the total velocity field at the upper and lower levels of the troposphere

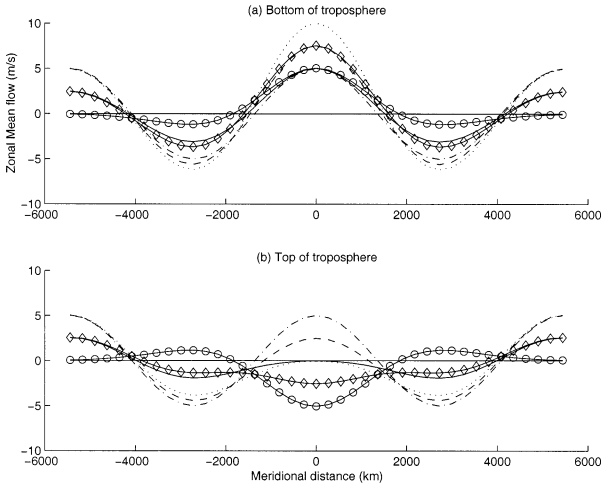

FIG. 1. Zonal mean velocities at (a) the bottom and (b) the top of the troposphere as a function of meridional coordinate for the examples described in Table 1 ($m = 1$). Circles correspond to the mean shears used in the nonlinear study of section 5a [$\overline{A}(0) = 5$, $\overline{B} = 0$ m s^{-1}] whereas diamonds correspond to the nonlinear study of section 5b [$\overline{A}(0) = 5$, $\overline{B} = 2.5$ m s^{-1}]. The curves with no symbols correspond to the cases in Table 1: $\overline{A}(0) = 0$, $\overline{B} = 0$ m s^{-1}, solid; $\overline{A}(0) = 0$, $\overline{B} = 5$ m s^{-1}, dot–dash; $\overline{A}(0) = 2.5$, $\overline{B} = 5$ m s^{-1}, dashed; $\overline{A}(0) = 2.5$, $\overline{B} = 2.5$ m s^{-1}, solid; $\overline{A}(0) = 5$, $\overline{B} = 5$ m s^{-1}, dotted.

is displayed for various vertical and horizontal zonal mean shears compatible with both the asymptotics in (3.5) and the dimensional scales in (2.4). For the specific values of α, β, and γ derived later in the asymptotic procedure, it can be shown that $\alpha = \beta = \gamma$ for all m and, therefore, both $\overline{A}$ and $\overline{B}$ are conserved in time. With the previous information, the reader interested only in the physical implications of the reduced equations can jump immediately to sections 4 and 5.

b. Derivation of the asymptotic model

The asymptotic expansion from (3.5) is inserted into the LWSEBB equations in (2.9), (2.10) with $\delta^2 = \epsilon$ and successive powers of ϵ are required to vanish without secular behavior in time. As a consequence of the linear wave properties in (3.1) and (3.2) the terms of order ϵ automatically vanish. To consider the terms of order ϵ^2, the Riemann invariants, q and r, given in terms of $p_{\rm BC}$, $u_{\rm BC}$ by $q = (u + p)/\sqrt{2}$, $r = (u - p)/\sqrt{2}$, are introduced (Heckley and Gill 1984). The expansion of the baroclinic wave dynamics in (2.9) with (3.5) and $\delta^2 = \epsilon$ yields the following equations at order ϵ^2

$$q_{2,t} + q_{2,x} + L_- v_2 = -q_{1,\tau} - (\psi_{1,x}q_{1,y} - \psi_{1,y}q_{1,x}) + \frac{1}{\sqrt{2}}\left[\left(\frac{q_1 + r_1}{\sqrt{2}}\right)\psi_{1,xy} + v_1\psi_{1,yy}\right]$$

$$r_{2,t} - r_{2,x} - L_+ v_2 = -r_{1,\tau} - (\psi_{1,x}r_{1,y} - \psi_{1,y}r_{1,x}) + \frac{1}{\sqrt{2}}\left[\left(\frac{q_1 + r_1}{\sqrt{2}}\right)\psi_{1,xy} + v_1\psi_{1,yy}\right]$$

$$L_+ q_2 - L_- r_2 = -v_{1,t} \tag{3.8}$$

with $L_\pm$ the raising and lowering operators, $L_\pm = 1/\sqrt{2}(d/dy \pm y)$, $\psi_1 = -B\sin(ly)$, and q_1, r_1 calculated from the leading-order baroclinic terms in (3.5).

Recall that the amplitudes of the first-order barotropic and baroclinic modes are waves traveling at the same speed so they will resonate with the linear operator at second-order generating secular terms. Such secular terms arise from the forcing functions on the right-hand side of (3.8), which generate a response of order $\epsilon^2 t = \epsilon\tau$, which would be the same strength as the leading-order terms in the analysis. On the other hand, the goal is to incorporate all of the nonlinear dynamics to leading order self-consistently in the first-order terms (see Majda and Klein 2003; Majda 2003, for other examples). Thus the secular terms are required to vanish. This is achieved by requiring that the projection of the equations in (3.8) onto the eigenfunctions of the adjoint linear problem defined by the left-hand side of (3.8) must vanish. However, the linear operator is skew self-adjoint meaning that the adjoint eigenfunction is equal to the eigenfunction itself. The projection is accomplished by recognizing that the integral over the domain of the inner product of the equations in (3.8) with

$$\begin{bmatrix} -\dfrac{1}{(m+1)}D_{m+1}(y)\phi(x) \\ D_{m-1}(y)\phi(x) \\ -\left(\dfrac{2}{2m+1}\right)D_m(y)\dfrac{\partial}{\partial x}\phi(x) \end{bmatrix} \equiv \begin{bmatrix} \hat{q}(y)\phi(x) \\ \hat{r}(y)\phi(x) \\ \hat{v}(y)\dfrac{\partial}{\partial x}\phi(x) \end{bmatrix} \tag{3.9}$$

must vanish for arbitrary $\phi(x)$; this relation also defines the eigenfunctions $\hat{q}(y)$, $\hat{r}(y)$, $\hat{v}(y)$. On performing this multiplication and integrating by parts to remove derivatives on $\phi(x)$, the first asymptotic equation in (3.6) emerges with explicit coefficients r_A, D_A, α, β given by

$$r_A = \int_{-\infty}^{\infty} (\hat{q}^2 + \hat{r}^2)\, dy, \qquad D_A = \frac{1}{2m+1}\int_{-\infty}^{\infty} \hat{v}^2\, dy$$

$$\alpha = -\int_{-\infty}^{\infty}\left[l^2\sin(ly)\frac{\hat{v}}{\sqrt{2}}(\hat{q}+\hat{r}) - l\cos(ly)(\hat{q}^2+\hat{r}^2)\right]dy$$

$$\beta = \int_{-\infty}^{\infty} l\cos(ly)(\hat{q}^2 + \hat{q}\hat{r} + \hat{r}^2)\, dy. \tag{3.10}$$

The derivation of the second equations in (3.6) for the barotropic mode is similar to the previous. The equation for the barotropic mode at second order becomes

$$\psi_{2yyt} + \psi_{2x} = -l^2 B_\tau \sin(ly) + B_{xxt}\sin(ly) + (u_1)_{xy}^2 + (u_1 v_1)_{yy}. \tag{3.11}$$

Once again, due to the resonance condition in (3.3), the right-hand side of (3.11) contains potential secular terms, which must be removed. With (3.3) it is easy to see that no secular terms arise provided that the forcing term has a zero projection on $\sin(ly)$. Thus, multiplying (3.11) by $\sin(ly)$ and integrating in y results in the second asymptotic equation in (3.6) with the explicit coefficients

$$r_B = l^2\frac{L_*}{2}, \qquad D_B = \frac{1}{l^2}\frac{L_*}{2}$$

$$\gamma = \int_{-\infty}^{\infty}\left[l\cos(ly)(\hat{q}+\hat{r})^2 + l^2\sin(ly)\frac{\hat{v}}{\sqrt{2}}(\hat{q}+\hat{r})\right]dy. \tag{3.12}$$

With (3.10) and (3.12) it is straightforward but tedious to verify explicitly that $\alpha - 2\beta + \gamma = 0$, which is needed for the conservation of energy in (3.7). Also tedious is the evaluation of the coefficients that yields $\alpha = \beta = \gamma$ for all values of m and implies that the zonal mean vertical ($\overline{A}$) and meridional ($\overline{A}$, $\overline{B}$) shears are constants of (3.6).

4. Properties of the reduced equations

Here the basic properties of the reduced equations in (3.6) are developed. It is convenient to rescale space, time, and the nonlinear amplitudes so that the equations in (3.6) have the canonical form

$$A_\tau - DA_{xxx} + BA_x + AB_x = 0$$
$$B_\tau - B_{xxx} + AA_x = 0. \tag{4.1}$$

The elementary but tedious reduction of (3.6) to the canonical form in (4.1) having only the single parameter, D is presented in the appendix in order to streamline the discussion here. Note that the amplitudes, A and B in (4.1), are given the same notation as in (3.5) although they are actually rescaled multiples of those amplitudes. The values of the coefficient, D in (4.1), for the various equatorial Rossby waves are

$$m = 1, \quad D = 0.889$$
$$m = 2, \quad D = 0.960$$
$$m = 3, \quad D = 0.980. \tag{4.2}$$

Since the interest for (3.6) is planetary waves that move in the east–west direction, periodic boundary conditions in the x-variable for both A and B are assumed here. It is convenient to split A and B into zonal means, which from (4.1) are conserved in time, plus wave fluctuations,

$$A = \overline{A} + A'(x,\tau), \qquad B = \overline{B} + B'(x,\tau). \tag{4.3}$$

As in (3.6), (3.7) the equations in (4.1) conserve the total energy, $E = 1/2\int (A^2 + B^2)$, but, as shown below, there is nontrivial exchange of energy between the barotropic waves, B', and the baroclinic waves, A', promoted by a nonzero baroclinic mean shear, $\overline{A} \neq 0$. Furthermore, with the expansion in (3.5), (2.3) and the rescaling transformation in the appendix, one readily

computes that, in the vicinity of the equator and for $m = 1$,

$B' > 0$ corresponds to cyclonic barotropic flow,

$A' > 0$ corresponds to (anti-) cyclonic baroclinic flow at the bottom (top) (4.4)

with negative signs in (4.4) yielding anticyclonic flows. Furthermore, associated with the baroclinic waves is a flow divergence or convergence in the plane, which is of opposite sign at the top and bottom of the troposphere. It is straightforward to see that evaluating the convergence (divergence) at the equator yields

$A'_x > 0$ corresponds to divergence (convergence) at the bottom (top) of the troposphere,

$A'_x < 0$ corresponds to convergence (divergence) at the bottom (top) of the troposphere. (4.5)

a. Energy transfer between the waves

In the rescaled equations, $1/2 \int A'^2$ represents the energy in the baroclinic waves while $1/2 \int B'^2$ represents the energy in the barotropic waves. Straightforward manipulations of (4.1) give the following explicit formulas for the rate of change of the barotropic and baroclinic wave energy in time

$$\left(\int \frac{B'^2}{2}\,dx\right)_\tau = -\left(\int \frac{A'^2}{2}\,dx\right)_\tau = \frac{1}{2}\int (A')^2 B'_x\,dx + \frac{1}{2}\int \overline{A}(A'B'_x - B'A'_x)\,dx. \quad (4.6)$$

This formula reveals that the spatial structure of $(A')^2B'_x$ and $A'B'_x - B'A'_x$ in a given solution controls the flux of energy among the barotropic and equatorial baroclinic waves. Furthermore, the role of baroclinic mean shear in enhancing energy transfer between the barotropic and equatorial baroclinic waves is explicitly seen in the second term in (4.6). It is straightforward to show that maxima of $A'B'_x - B'A'_x$ correspond to either a coincidence in the zonal direction of a barotropic cyclone pair near the equator with baroclinic convergence at the bottom of the troposphere or a barotropic anticyclone pair near the equator with baroclinic divergence at the bottom of the troposphere. Conversely, the minima correspond to coincidences of barotropic cyclones with divergence or barotropic anticyclones with convergence at the bottom of the troposphere.

b. Linear theory for zonal mean shear states

Equation (4.1) has exact solutions, $A(x, \tau) = A$, $B(x, \tau) = \overline{B}$, with $\overline{A}$, $\overline{B}$ prescribed constants that correspond to vertically and horizontally varying mean shears according to (3.5) and Fig. 1. The linearized equations about these constant states for perturbations, a, b, $A = \overline{A} + a(x, \tau)$, $B = \overline{B} + b(x, \tau)$, are

$$a_\tau - Da_{xxx} + \overline{B}a_x + \overline{A}b_x = 0$$
$$b_\tau - b_{xxx} + \overline{A}a_x = 0. \quad (4.7)$$

Special solutions of (4.7) with the form $(a, b)^T = \exp[ik(x - c_\pm(k)\tau)]\mathbf{e}_\pm$ have the explicit formula for the wave speed $c_\pm(k)$,

$$c_\pm(k) = \frac{\overline{B} + k^2(1 + D)}{2} \pm \frac{\sqrt{[k^2(1 - D) - \overline{B}]^2 + 4\overline{A}^2}}{2}. \quad (4.8)$$

Furthermore, the angle of the barotropic to the baroclinic component of the associated eigenvector, $M^\pm_{\mathrm{BT,BC}}$, is given by

$$M^\pm_{\mathrm{BT,BC}} = \frac{2}{\pi}\arctan\left[\frac{|c_\pm(k) - 2k^2D - 2\overline{B}|}{2|\overline{A}|}\right] \quad (4.9)$$

unless $\overline{A} = 0$, in which case the equations in (4.7) decouple into separate equations for the barotropic and baroclinic modes so that $M^+_{\mathrm{BT,BC}} = 1$ and $M^-_{\mathrm{BT,BC}} = 0$. Note that $M^\pm_{\mathrm{BT,BC}} \to 1$ reflects a dominant barotropic component of the linearized mode while $M^\pm_{\mathrm{BT,BC}} \to 0$ reflects a dominant baroclinic component. The elementary stability theory just derived is the analogue for the model of that presented in Wang and Xie (1996) for specific horizontally and vertically varying zonal shears at large scales. This is shown later.

PHYSICAL INTERPRETATION OF THE WAVES AND LINEAR THEORY

For the physical interpretation of the solutions of Eqs. (3.6) or the normalized version in (4.1), one needs to unravel the two basic scalings in (2.7) and (3.5) using the distinguished limit $\delta^2 = \epsilon$ with the dimensional units in (2.4). First, as discussed earlier following (3.7), the conservative choice of $\epsilon = 0.1$ allows for reasonable zonal barotropic and baroclinic velocities of order 5 m s^{-1} yielding $\delta = 0.316$. With (2.8) and this choice for ϵ, variations in x are allowed over the length scale $L = \delta^{-1}L_E \approx 5000$ km so that with the equatorial circumference $\approx$40 000 km as the basic outer-length scale, $L_{\max}$, the first eight wavenumbers, $1 \le n \le 8$ where $k \equiv 2\pi n/L_{\max}$ have direct physical significance. Also note from (2.8) that the physical meridional velocities in the theory are weaker than the zonal velocities by the factor δ, which yields magnitudes of order 1.4 m s^{-1}, while meridional variation of all physical quantities is allowed on the scale of $L_E = 1500$ km. The units of time τ in (3.6) are related to $T_E = 8$ h from (2.4) by $\tau = (\epsilon\delta)^{-1}T_E$

TABLE 1. Wave speeds (in m s^{-1}) and angles of eigenvectors.

Mean flow	$n = 1$, $L = 10$		$n = 2$, $L = 20$		$n = 3$, $L = 13.3$		$n = 4$, $L = 10$	
BT speed	C_+	C_-	C_+	C_-	C_+	C_-	C_+	C_-
BC speed	M^+	M^-	M^+	M^-	M^+	M^-	M^+	M^-
0	−16.4	−16.4	−15.5	−15.6	−14.0	−14.3	−11.9	−12.4
0	1.0	0.0	1.0	0.0	1.0	0.0	1.0	0.0
0	−14.9	−17.9	−14.1	−17.1	−12.6	−15.6	−10.6	−13.7
5	0.50	0.50	0.51	0.49	0.53	0.47	0.56	0.44
5	−14.4	−16.4	−13.6	−15.5	−12.3	−14.0	−10.4	−11.9
0	0.00	1.00	0.00	1.00	0.00	1.00	0.00	1.00
5	−14.2	−16.7	−13.3	−15.8	−12.0	−14.3	−10.1	−12.2
2.5	0.21	0.79	0.21	0.79	0.23	0.77	0.25	0.75
2.5	−14.3	−17.5	−13.5	−16.6	−12.1	−15.2	−10.1	−13.1
5	0.40	0.60	0.41	0.59	0.43	0.57	0.45	0.55
2.5	−15.0	−16.8	−14.2	−15.9	−12.8	−14.4	−10.8	−12.41
2.5	0.32	0.68	0.33	0.67	0.36	0.64	0.40	0.60
5	−13.6	−17.2	−12.8	−16.3	−11.4	−14.9	−9.4	−12.8
5	0.31	0.69	0.32	0.68	0.33	0.67	0.35	0.65

Total wave speeds, $C_\pm = c\,(c_m + \epsilon\tilde{c}_\pm)$ for a selection of barotropic and baroclinic mean flows for the case $m = 1$. Speeds are measured in m s^{-1}; wavelengths, L, are measured in 1000 km. Normalized angles, $M^\pm_{BT,BC}$, from (4.9): 0 = baroclinic, 1 = barotropic.

yielding a basic unit of time of roughly 11 days for solutions of (3.6). It is worth remarking here that the unit of time for the validity of the basic idealized equations in (3.6) fits nicely with the time of roughly 12 days observed by Hoskins and Jin (1991) in their numerical studies, where the onset of midlatitude baroclinic instability of the transient waves eventually develops. Finally, observe that with (3.5) and the longer timescale, $\tau = \epsilon t$, for (3.6), a wave moving with phase speed $\tilde{c}$ for the equations in (3.6) shifts the basic wave speed, c_m in (3.3), (3.5) by $\epsilon\tilde{c}$ resulting in the dimensional-shifted physical wave speed

$$c(c_m + \epsilon\tilde{c}). \tag{4.10}$$

With (2.4), $c\,c_m \approx -16.7$ m s^{-1}, the shifts in this wave speed are 5 m $s^{-1} \times \tilde{c}$ so that comparatively small changes in the phase speed in solutions of (3.6) can imply fairly large departures dimensionally from the equatorial Rossby wave speed.

Next, the physical interpretation of the results from linear theory in (4.7), (4.8), (4.9) is presented for the rescaled version of (3.6) in (4.1). First note from (4.2) that the wave speeds $c_\pm(k)$ in (4.8) are always real for all m; zonally constant shears are never unstable in this model. Here, as in Wang and Xie (1996), the focus for the linear theory is on the structure of the $m = 1$ modes with the dimensional parameters in (2.4) with various combinations of barotropic and baroclinic zonal mean shears, which are obtained by varying $\overline{A}$ and $\overline{B}$. The physical interpretation of the linear stability theory about a variety of basic zonal shear flows for $m = 1$ is summarized in Table 1; there, the relative magnitude of the barotropic and baroclinic components, $M^\pm_{\mathrm{BT,BC}}$, and the physical total wave speeds, still denoted $c_\pm$, utilizing (4.10) are reported for planetary-scale wavenumbers, $n = 1, 2, 3, 4$ for various combinations of baroclinic and barotropic mean shears consistent with the asymptotics. First note the strongly coupled equatorial baroclinic–barotropic linear waves that occur for the case with the purely baroclinic zonal mean shear $\overline{A} = 5$ m s^{-1}, $\overline{B} = 0$, with significant phase speed shifts compared with $c_m = -16.7$ m s^{-1} for the wavelengths of order 10 000 km. This contrasts with the complete lack of barotropic and baroclinic mode coupling at all wavenumbers for the purely barotropic zonal mean shear with $\overline{A} = 0$, $\overline{B} = 5$ m s^{-1}, although this case also has strong phase shifts in the wave speeds due to both dispersion and barotropic advection as can be anticipated from (4.8), (4.9). The remaining cases with combinations of baroclinic and barotropic mean shear involve a mixture of the two effects that are prominent in the two cases discussed here. Although not displayed here for lack of space, the actual linear modes with vertical mean shear and various barotropic mean shears have a strong physical resemblance to the wave structures reported in Figs. 8 and 14 in Wang and Xie (1996). This is evident from the values of $M^\pm_{\mathrm{BT,BC}}$ in Table 1 for these cases combined with the physical structure of both the barotropic and baroclinic waves given in (3.5). Also note that the strongly coupled barotropic–baroclinic phase speeds reported in Table 1 with various mean shears fit nicely with the trends reported by Hoskins and Jin (1991); their simulations have $c = 41$ m s^{-1} and linear long-wave first baroclinic equatorial Rossby wave speeds of −13.7 m s^{-1}, but observed long-wavelength equatorial baroclinic–barotropic wave packets in the simulations with the reduced phase speeds −8 m s^{-1}. Finally, Wang and Xie (1996) have established the important fact that linear theory for the equatorial β-plane equations in this long-wave regime is an excellent approximation to similar waves in spherical geometry provided vanishing normal flow boundary conditions are imposed on boundaries $y = \pm L$ with $L \approx 4L_E$. With (3.4) for $m = 1$ and (3.5), the barotropic mode identically satisfies the boundary conditions at $y = \pm 3.6\ L_E$, while the equatorial baroclinic mode has negligible meridional veloc-

ities at $y = \pm 3.6L_E$. Thus, the basic linear and nonlinear wave theories developed here also apply to the situation with spherical geometry.

5. Nonlinear dynamics for the reduced model

Here the simplified asymptotic equations in (3.6) for $m = 1$ are utilized to gain insight into the transient exchange of energy between midlatitude barotropic Rossby waves and equatorial baroclinic Rossby waves. For these purposes, the rescaled equations in (4.1) are integrated numerically for a variety of initial data. A standard de-aliased pseudospectral method with 64 modes is utilized for the spatial discretization of (4.1) and combined with fourth-order Runge–Kutta time discretization as the basic numerical method. Conservation of energy within 10^{-4}% is satisfied for all numerical solutions reported later and the numerical code was validated initially by reproducing the linear theory for small perturbations of mean shears described earlier in section 4. The basic physical regime for the parameters here is given by the value $c = 50$ m s^{-1} for the basic equatorial wave speed from (2.4) with $m = 1$ and the choice $\epsilon = 0.1$. Thus, the physical interpretation of the waves described in section 4 will be used here to quantify results of the integration of (4.1). In particular, recall that only roughly the first eight zonal wavenumbers in the solution of the reduced model in (4.1) have direct physical significance for these parameter values, so it is important to derive tests of the numerical solution to insure that significant energy is not transferred to large zonal wavenumbers, n, with $|n| > 8$ on the time interval of interest; if significant transfer to small scales occurs, the solutions of (4.1) automatically lose their physical significance. The test utilized here is to monitor in time whether the summed contributions in all zonal wavenumbers with $|n| > 8$ exceeds 4% of the (conserved) total energy. In all of the numerical experiments reported later wave energy was supplied initially only in the first four wave numbers, $1 \leq n \leq 4$ with statistically identical random amplitudes and phases for all four wavenumbers and, in dimensional terms, with the constraint that the square roots of the total mean wave energy does not exceed 5 m s^{-1} in order to be consistent with the amplitude value $\epsilon = 0.1$ in (3.5). Surprisingly, the solutions of the reduced equations with such initial data passed the test for validity for arbitrarily long integrations in time with ease; a typical spectral distribution for these simulations is presented in Fig. 2 where a logarithmic vertical scale is employed to show the rapid falloff of spectral amplitude for wavenumbers with $|n| \leq 8$. Various aspects of the solutions of (4.1) will be shown over 100 days to illustrate general trends; however, the detailed structure of these solutions will only be discussed for times less than 15 days since other physical effects such as midlatitude baroclinic instability develops from such transient wave packets in roughly 12 days (Hoskins and Jin 1991).

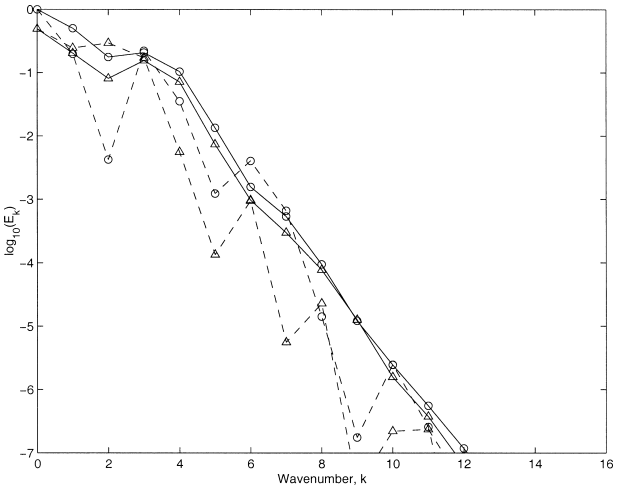

FIG. 2. Typical energy spectrum showing rapid decay with wavenumber for the example discussed in section 5b: $\overline{A}(0) = 5$, $\overline{B} = 2.5$ m s^{-1}. Dashed curves are the instantaneous spectra, solid curves are time-averaged spectra. Circles are the baroclinic amplitudes, *A*; diamonds are the barotropic amplitudes, *B*. Wave amplitudes, energies, and energy fluxes in all of the figures have been scaled to the normal form given in the text.

a. The transfer of energy from barotropic Rossby waves to equatorial baroclinic Rossby waves

Here the initial data for the waves always consists of a random distribution of barotropic Rossby waves as described earlier with zero energy initially in the baroclinic Rossby waves. First, as remarked earlier in section 3, if there is zero mean baroclinic shear then for solutions of (4.1) it is impossible to have nonzero energy in the equatorial waves at any later time. Therefore, an initial equatorial baroclinic mean shear is necessary to have any possibility of energy transfer to the baroclinic waves in (4.1). Thus, initially a wide variety of nonzero barotropic and baroclinic zonal mean shears were prescribed at time $t = 0$ with the same range of values as given in Table 1. The time history over 100 days of the square root of the barotropic and baroclinic wave energy, scaled to correspond to Eq. (4.1) is depicted in Fig. 3 for various mean shears and representative random barotropic waves; many other simulations with initially random barotropic waves with fixed zonal mean shears were performed. The first three cases all display the rapid conversion on the order of 15 days of significant barotropic wave energy to baroclinic wave energy; this is the typical robust behavior in the transfer of energy; the random initial data in these cases is characterized by a few isolated coherent barotropic Rossby waves. The detailed dynamics of the first case is described later. In the example in Fig. 3d for $\overline{A} = 2.5$ m s^{-1}, $\overline{B} = 5$ m s^{-1}, the random initial data for the barotropic mode had only weak-amplitude coherent waves and significant transfer required unphysical times on the order of several months. On the other hand, the random initial data for the case with $\overline{A} = 2.5$ m s^{-1}, $\overline{B} = 2.5$

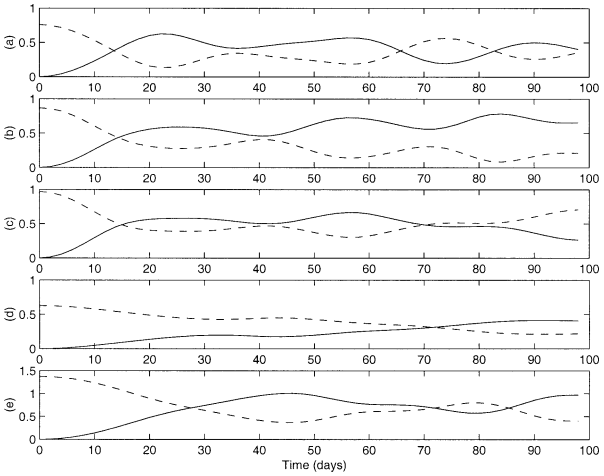

FIG. 3. The transfer of barotropic wave energy to baroclinic wave energy for $m = 1$: at $t = 0$ all cases have $|A'|^2 = 0$. Barotropic wave energy (dashed curves); baroclinic wave energy (solid curves). (a) $\overline{A}(0) = 5$, $\overline{B} = 0$ m s^{-1}; (b) $\overline{A}(0) = 5$, $\overline{B} = 2.5$ m s^{-1}; (c) $\overline{A}(0) = 5$, $\overline{B} = 5$ m s^{-1}; (d) $\overline{A}(0) = 2.5$, $\overline{B} = 5$ m s^{-1}; (e) $\overline{A}(0) = 2.5$, $\overline{B} = 2.5$ m s^{-1}.

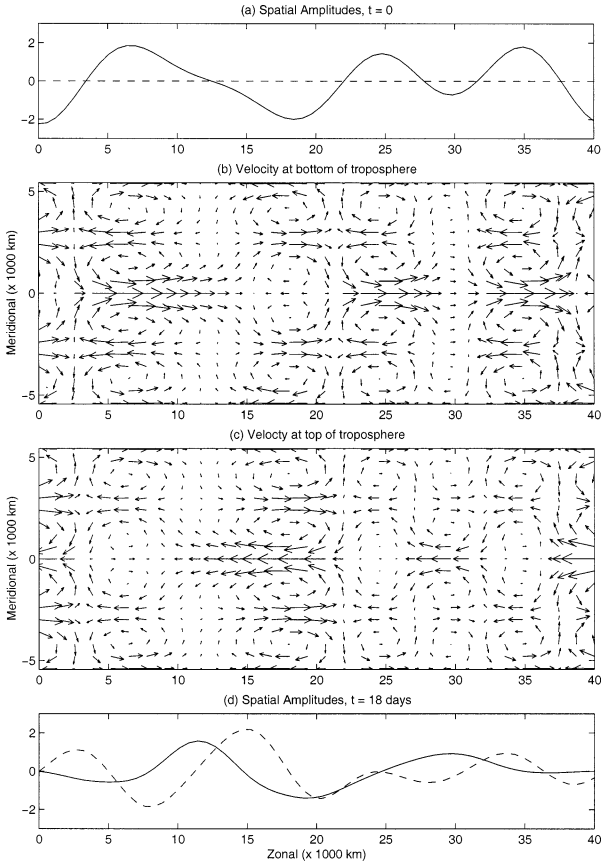

FIG. 4. Nonlinear evolution of amplitude equations with zero baroclinic wave energy initially, $\overline{A}(0) = 5$, $\overline{B} = 0$ m s^{-1}. (a) Initial wave amplitudes: $A'(x, 0)$ (dashed); $B'(x, 0)$ (solid). Velocity at (b) the bottom and (c) the top of the troposphere as a function of meridional and zonal coordinate at $t = 0$. (d) Wave amplitudes at $t = 18$ days: $A'(x, 0)$ (dashed); $B'(x, 0)$ (solid).

m s^{-1}, in Fig. 3e consisted of a coherent Rossby wave train over the entire 40 000-km domain and the rate of energy transfer to the equatorial baroclinic Rossby waves was reduced.

Details of the energy transfer from barotropic to equatorial baroclinic waves are shown in Figs. 4, 5, and 6 for times $t = 0$, 10, and 14 days for the representative case in Fig. 3a with $\overline{A} = 5$, $\overline{B} = 0$ m s^{-1}. Here and later, the wave patterns are shown relative to a reference frame moved at the resonant wave speed -16.7 m s^{-1}. The spatial structure of the amplitudes of the waves, A', B', as well as the spatial structure of the energy flux terms, $\overline{A}(A'B'_x - B'A'_x)$ and $|A'|^2B'$, from (4.6) are displayed at each time after the initial. Furthermore, local maxima in the divergence and convergence of the baroclinic flow are shown at the bottom of the troposphere and in the plot of the wave amplitudes.

Recall from (4.6) that the average of $\overline{A}(A'B'_x - B'A'_x)$ controls the flux of energy through coupling provided by the baroclinic mean shear while $|A'|^2B'$ is the energy flux through wave–wave coupling alone. Figure 4a shows the initial data with coherent barotropic Rossby waves at time $t = 0$ while in Fig. 4d the amplitude of the equatorial baroclinic and barotropic Rossby waves that develop at time $t = 18$ days is shown. At this time the solution is clearly dominated by coherent localized equatorial baroclinic wave activity. The leftmost barotropic equatorial cyclone pair depicted in Figs. 4a,b,c at time $t = 0$ is important for this process. The route of this strong energy transfer to equatorial baroclinic waves is shown through the snapshots in Figs. 5 and 6. By the time $t = 10$ days as depicted in Fig. 5 this barotropic equatorial cyclone pair has created significant localized baroclinic wave activity with visible lower-level baroclinic velocity divergence slightly behind the barotropic wave, and lower-level baroclinic velocity convergence ahead of the wave in a region of anticyclonic barotropic flow. As seen from (4.6) these two mechanisms both cause the instantaneous depletion of barotropic wave energy over the local region of the composite wave as shown in Fig. 5b. On the other hand, the energy flux contribution from $|A'|^2B'_x$ has a dipolar structure in the composite wave with production of negative values of $|A'|^2B'_x$ yielding equatorial baroclinic energy ahead of the Rossby wave as evidenced from the formula in (4.6); the strong local baroclinic structure is clearly visible in the upper- and lower-level velocity profiles in Fig. 5. Furthermore, according to (4.6) the positive part of the local dipolar structure in $|A'|^2B'_x$ in the vicinity of the barotropic Rossby wave reinforces the energy in this barotropic wave to partially compensate for the local depletion. As shown in Fig. 6 for the time $t = 14$ days, all of the same physical processes just discussed continue to reinforce each other and amplify the equatorial baroclinic lower-level cyclone pair. This mechanism of energy transfer clearly has the structure of a ''westerly wind burst''; also note that the wave

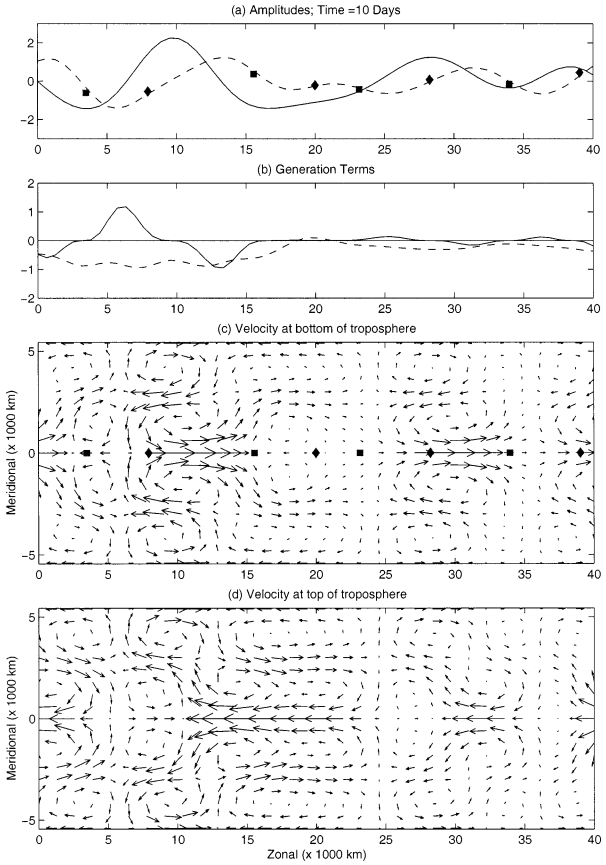

FIG. 5. Nonlinear evolution of amplitude equations with zero baroclinic wave energy initially. (a) Wave amplitudes at $t = 10$ days: $A'(x)$ (dashed); $B'(x)$ (solid). (b) Wave energy flux density: $(1/2)(A')^2 B'_x$ (solid); $(1/2)\overline{A}(A'B'_x - B'A'_x)$ (dashed). Corresponding velocity field at (c) the bottom and (d) the top of the troposphere. In (a) and (c) squares (diamonds) correspond to local maxima of the convergence (divergence) at the bottom of the troposphere.

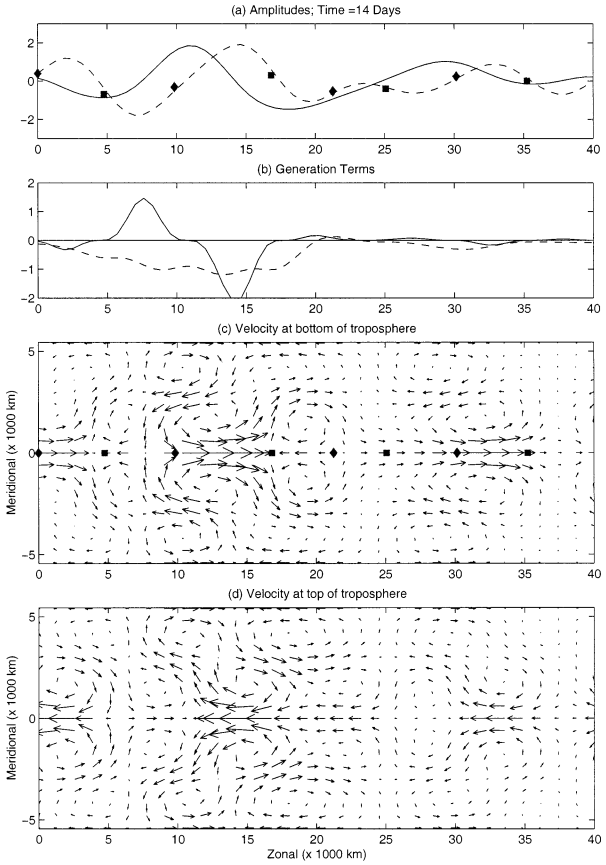

FIG. 6. The same as in Fig. 5 except (a) wave amplitudes at $t = 14$ days.

propagates eastward relative to the background resonant wave speed (Hoskins and Jin 1991).

In Figs. 4–6, the zonal mean baroclinic flow is westerly at low levels and there is no barotropic mean flow. What happens with the same purely barotropic initial data in a zonal mean baroclinic shear with the same strength that is easterly at low levels? This is readily understood through the information already presented in Figs. 4, 5, and 6. First, the asymptotic equations in (4.1) respect the symmetry that if (A, B) is a solution then $(-A, B)$ is also a solution while the initial data $(-A, B)$ at time $t = 0$ from Fig. 4 corresponds to the same barotropic initial data in an easterly lower-level baroclinic shear. Thus, with (2.3) the solution in Figs. 4, 5, and 6 automatically yields the solution with an easterly mean shear with the correspondence that the upper- (lower) level flow in Figs. 4–6 correspond to the lower- (upper) level flow in the case of an easterly low-level baroclinic mean. With this interpretation of Figs. 4–6, it is evident that strong low-level baroclinic convergence develops to the west of the baroclinic Rossby wave through an ''easterly wind burst mechanism'' in the asymptotic model. Note that boundary layer dissipation will break this symmetry between westerly and easterly baroclinic mean shear in an interesting fashion, which should be explored in the future.

b. *The transfer of energy from equatorial baroclinic Rossby waves to barotropic Rossby waves*

Here, the initial data for waves always consists of a random distribution of equatorial baroclinic Rossby waves as described earlier with zero energy initially in the barotropic waves. The time history of the energy in the waves and the baroclinic mean shear over 100 days for representative random initial data is given in Fig. 7 for five representative cases with various mean zonal shears. The first three cases in Figs. 7a,b,c have nonzero baroclinic mean shear and random initial data with coherent localized equatorial Rossby waves; there is rapid transfer of baroclinic wave energy within 15 days to barotropic Rossby waves. The case in Fig. 7d with the same vertical shear as in Fig. 7c had lower wave energy with no coherent localized Rossby waves and a much weaker midlatitude response emerges. Finally, the last case in Fig. 7e has only barotropic mean shear, so $\overline{A} =$

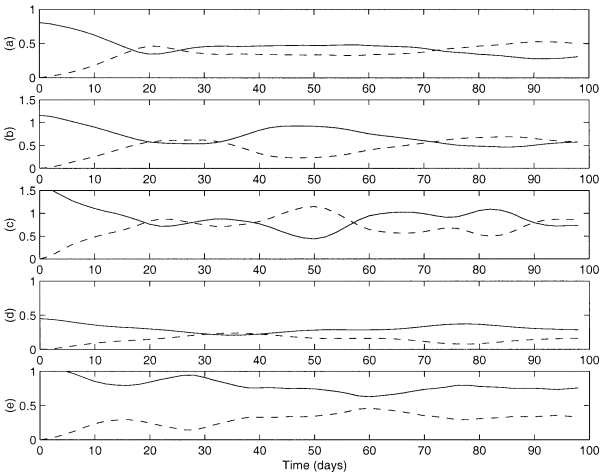

FIG. 7. The transfer of baroclinic wave energy to barotropic wave energy for $m = 1$: at $t = 0$ all cases have $|B'|^2 = 0$. Barotropic wave energy (dashed curves); baroclinic wave energy (solid curves). (a) $\overline{A}(0) = 5$, $\overline{B} = 0$ m s^{-1}; (b) $\overline{A}(0) = 2.5$, $\overline{B} = 5$ m s^{-1}; (c) $\overline{A}(0) = 5$, $\overline{B} = 2.5$ m s^{-1}; (d) $\overline{A}(0) = 2.5$, $\overline{B} = 5$ m s^{-1}; (e) $\overline{A}(0) = 0$, $\overline{B} = 5$ m s^{-1}.

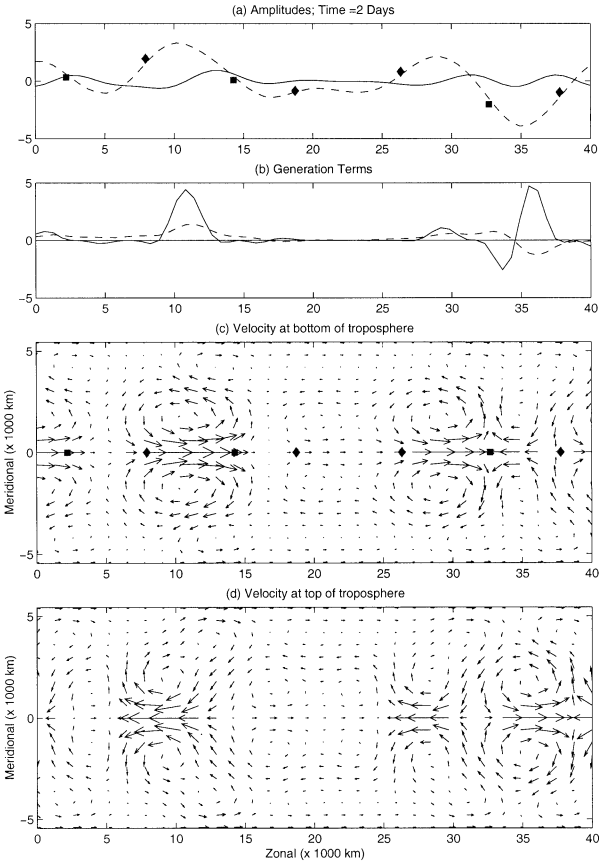

FIG. 8. Nonlinear evolution of amplitude equations with zero barotropic wave energy initially. $\overline{A}(0) = 5$, $\overline{B} = 2.5$ m s^{-1}. (a) Wave amplitudes at $t = 2$ days: $A'(x)$ (dashed); $B'(x)$ (solid). (b) Wave energy flux density: $(1/2)(A')^2B'_x$ (solid); $(1/2)\overline{A}(A'B'_x - B'A'_x)$ (dashed). Corresponding velocity field at (c) the bottom and (d) the top of the troposphere. In (a) and (c) squares (diamonds) correspond to local maxima of the convergence (divergence) at the bottom of the troposphere.

0; the midlatitude response is very weak in this case without baroclinic mean shear (Hoskins and Jin 1991). Details of the energy transfer from equatorial baroclinic to barotropic Rossby waves are shown in Figs. 8, 9, and 10 for the representative case in Fig. 7c with $\overline{A} = 5$ m s^{-1}, $\overline{B} = 2.5$ m s^{-1}.

In Fig. 8, two regions of localized equatorial baroclinic wave activity that existed initially, persist after 2 days. In Fig. 8b the same energy flux terms used earlier are plotted and indicate an overlapping localized region of barotropic energy production through both the direct wave coupling and the mean shear coupling located at the coherent leftmost equatorial baroclinic lower-level cyclone evident initially in Figs. 8a,c. As shown in Figs. 9 and 10 for the times $t = 8$ and $t = 14$ days, these mechanisms amplify and reinforce each other and lead to a strong midlatitude barotropic response through the coherent barotropic Rossby wave clearly evident in Fig. 10. Specifically, Fig. 9 shows a barotropic equatorial cyclone pair in a region of equatorial baroclinic surface convergence; on the other hand, the large amplitude of the localized baroclinic Rossby wave creates localized barotropic energy production through the flux term $|A'|^2B'_x$ in regions where B' increases. According to (4.6), both mechanisms strongly reinforce and lead to a localized increase in barotropic wave energy. Figure 10 indicates that the process continues in time.

Finally note that the time series in Figs. 3 and 7 over 100 days are representative of the complex and chaotic dynamics of general energy transfer among the waves and mean shear that occurs in general solutions of the reduced model.

6. Summary and conclusions

A reduced model has been derived here for the nonlinear interaction of long-wavelength equatorially trapped baroclinic Rossby waves and barotropic Rossby waves with a significant midlatitude projection. The model incorporates the nonlinear energy exchange between barotropic Rossby waves and baroclinic equatorial Rossby waves both through pure wave–wave coupling and enhanced by the presence of a baroclinic mean shear. Both the linear analysis from section 4 and the nonlinear studies in section 5 highlight the central role of baroclinic mean shear for sufficiently rapid nonlinear exchange of energy between the midlatitudes and the Tropics. The studies in section 5 reveal that the model includes a localized ''westerly wind burst'' mechanism, which allows for rapid energy transfer locally from barotropic to equatorial baroclinic waves. The basic case associated with dry gravity waves with a propagation speed of $c = 50$ m s^{-1} has been emphasized here. Composite barotropic/equatorial baroclinic Rossby waves are a prominent part of the observational record of the Tropics in regions of deep convection (Kiladis and Wheeler 1995); the simplest way to model deep con-

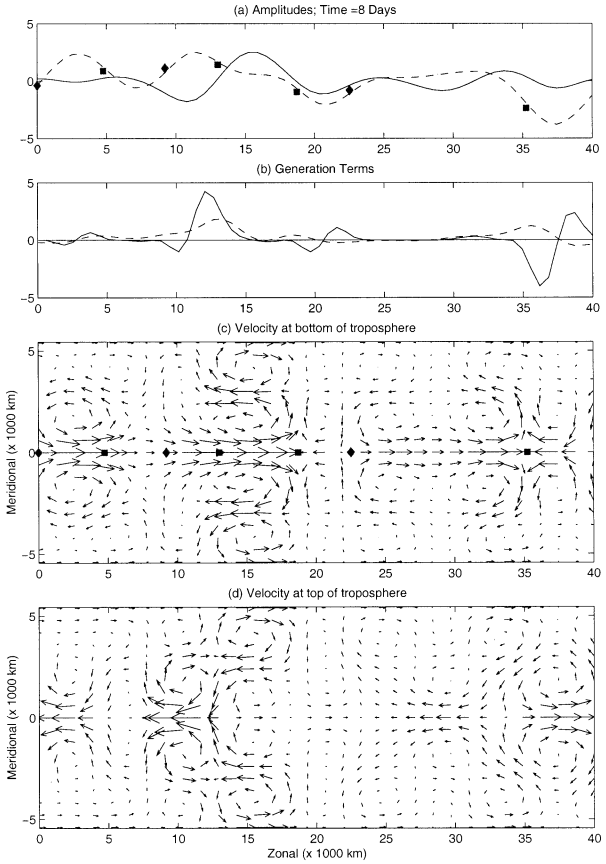

FIG. 9. Nonlinear evolution of amplitude equations with zero barotropic wave energy initially. (a) Wave amplitudes at $t = 8$ days: $A'(x)$ (dashed); $B'(x)$ (solid). (b) Wave energy flux density: $(1/2)(A')^2B'_x$ (solid); $(1/2)\overline{A}(A'B'_x - B'A'_x)$ (dashed). Corresponding velocity field at (c) the bottom and (d) the top of the troposphere. In (a) and (c) squares (diamonds) correspond to local maxima of the convergence (divergence) at the bottom of the troposphere.

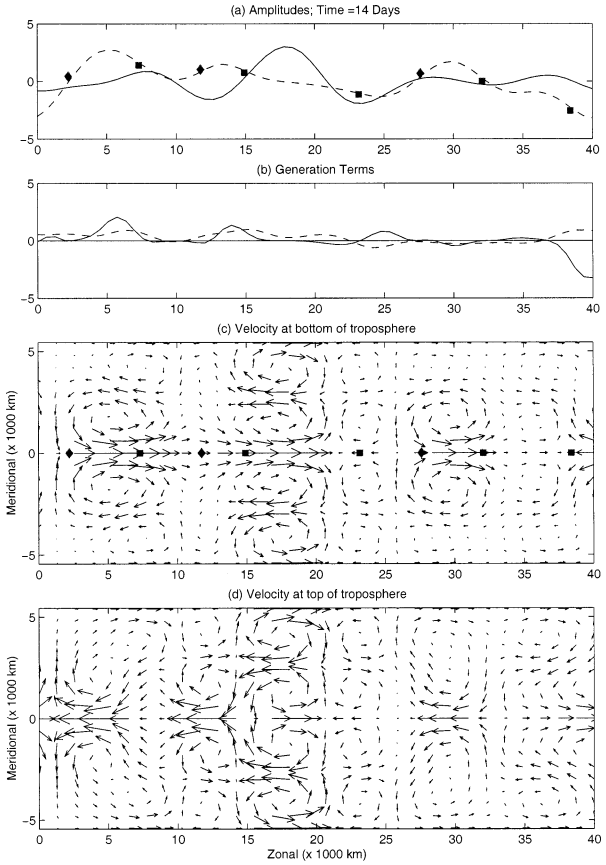

FIG. 10. The same as in Fig. 9 except (a) wave amplitudes at $t = 14$ days.

vection is to assume that it reduces the static stability in a dry model; thus, it would be interesting to test whether the nonlinear waves in section 5 from the model with $c \approx 15$ m s^{-1} have any of the structure of the observations of convectively coupled Rossby waves. Both dissipation and forcing are readily incorporated in the model and these are important additional effects that will be studied elsewhere by the authors. Recent scaling analysis (Majda and Klein 2003) reveals several other potential routes for midlatitude connections to the Tropics through resonant wave dynamics. The techniques developed here should be useful in these contexts. Another example involving resonance and nonlinear equatorial Kelvin waves has been developed recently (Majda et al. 1999).

The reduced equations derived in section 3 and analyzed in section 4 fit broadly into the class of coupled Korteueg-de Vries (KdV)-like equations, which occur through the interaction of resonant wave trains at long wavelengths but are novel in several aspects. Recently two KdV equations with linear coupling have been derived as weakly nonlinear models at long wavelengths for midlatitude baroclinic instability (Mitsudera 1994; Gottwald and Grimshaw 1999). The equations derived here are linearized KdV equations but more strongly coupled through quadratic nonlinearities, which are energy conserving; these novel quadratic nonlinearities play a central role in the westerly wind burst mechanism elucidated in section 5. The earlier-derived coupled KdV equations (Gottwald and Grimshaw 1999) for midlatitudes require weak β effect for their derivation while the present equatorial equations allow for order-one beta effect.

Obviously, simplified reduced equations describing multiwave interaction with both the $m = 1$ symmetric and $m = 2$ antisymmetric equatorial Rossby waves and suitable barotropic Rossby waves are very interesting as more realistic reduced models. Furthermore, the reduced models were derived here for the simplified vertical structure in section 2; the same derivation for a more complex vertical structure with $m = 1$ leads to the additional nonlinear term, $\mu(A^2)_x$, in the first equation in (3.6). All of these developments will be reported elsewhere by the authors in the future.

Acknowledgments. The research of A. J. Majda is partially supported by NSF Grant DMS-9972865, ONR Grant N0014-96-1-0043, and an NSF-FRG grant. J. A. Biello is supported by an NSF VIGRE Postdoctoral Fellowship, DMS-0083646.

APPENDIX

Rescaling the REEBBW

The normal form in (4.1) is derived from REEBBW in (3.6) through the following elementary rescalings. Substituting

$$A = A_0\hat{A}, \qquad B = s_B B_0 \hat{B},$$
$$x = x_0\hat{x}, \qquad \tau = \tau_0\hat{\tau}, \tag{A.1}$$

where $s_B = \pm 1$, into (3.6) yields (4.1) with the parameters (4.2) given by

$$1 + \kappa = \frac{\alpha}{\beta}, \qquad D = \frac{D_A r_B}{D_B r_A}. \tag{A.2}$$

It can be demonstrated that, upon evaluating the integrals that provide the nonlinear coupling, $\alpha = \beta = \gamma$ for all values of m. Therefore the time derivatives of the wave amplitudes are given by the zonal derivative of quadratic functions of these amplitudes. This ensures that both the barotropic and baroclinic zonal mean shears are constants in time.

Furthermore, the values of the scaling parameters, A_0, B_0, s_B, x_0, and τ_0 are chosen to be

$$A_0 = \frac{1}{\sqrt{r_A}}, \qquad B_0 = \frac{1}{\sqrt{r_A}},$$
$$x_0 = \sqrt{\frac{D_B r_A}{|\beta|\sqrt{r_B}}}, \qquad \tau_0 = \sqrt{\frac{D_B r_A^3 \sqrt{r_B}}{|\beta|^3}}, \tag{A.3}$$

where, in order to keep τ_0 positive the choice

$$s_B = \operatorname{sgn}(\beta) \tag{A.4}$$

must be made. The explicit values of the scaling parameters are

$$(A_0, B_0, x_0, \tau_0, s_B) = \begin{cases} (0.613, 0.429, 0.60, 1.97, 1) & \text{for } m = 1 \\ (0.531, 0.377, 0.60, 0.55, -1) & \text{for } m = 2. \end{cases} \tag{A.5}$$

REFERENCES

Boyd, J. R., 1980: Equatorial solitary waves. Part I: Rossby Solitons. *J. Phys. Oceanogr.,* **10,** 1699–1717.

Gottwald, G., and R. Grimshaw, 1999: The formation of coherent structures in the context of blocking. *J. Atmos. Sci.,* **56,** 3640–3662.

Heckley, W. A., and A. E. Gill, 1984: Some simple solutions to the problem of forced equatorial long waves. *Quart J. Roy. Meteor. Soc.,* **110,** 203–217.

Hoskins, B. J., and F.-F. Jin, 1991: The initial value problem for tropical perturbations to a baroclinic atmosphere. *Quart J. Roy. Meteor. Soc.,* **117,** 299–317.

——, and G.-Y. Yang, 2000: The equatorial response to higher latitude forcing. *J. Atmos. Sci.,* **57,** 1197–1213.

Kasahara, A., and P. L. Silva Dias, 1986: Response of planetary waves to stationary tropical heating in a global atmosphere with meridional and vertical shear. *J. Atmos. Sci,* **43,** 1893–1911.

Kiladis, G., and M. Wheeler, 1995: Horizontal and vertical structure of observed tropospheric equatorial Rossby waves. *J. Geophys. Res.,* **100,** 22 981–22 997.

Lim, H., and C. P. Chang, 1981: A theory for midlatitude forcing of tropical motions during winter monsoons. *J. Atmos. Sci.,* **38,** 2377–2392.

——, and ——, 1986: Generation of internal and external mode motions from internal heating: Effects of vertical shear and damping. *J. Atmos. Sci.,* **43,** 948–957.

Lin, J. W.-B., J. D. Neelin, and N. Zeng, 2000: Maintenance of tropical intraseasonal variability: Impact of evaporation–wind feedback and midlatitude storms. *J. Atmos Sci.,* **57,** 2793–2823.

Majda, A., 2003: *Introduction to PDE's and Waves for the Atmosphere and Ocean.* American Mathematical Society, 234 pp.

——, and M. Shefter, 2001: Models for stratiform instability and convectively coupled waves. *J. Atmos. Sci.,* **58,** 1567–1584.

——, and R. Klein, 2003: Systematic multiscale models for the Tropics. *J. Atmos. Sci.,* **60,** 357–372.

——, R. Rosales, E. Tabak, and C. Turner, 1999: Interaction of large-scale equatorial waves and dispersion of Kelvin waves through topographic resonance. *J. Atmos. Sci.,* **56,** 4118–4133.

Mitsudera, H., 1994: Eady solitary waves: A theory of type B cyclogenesis. *J. Atmos. Sci.,* **51,** 3137–3154.

Neelin, J. D., and N. Zeng, 2000: A quasi-equilibrium tropical circulation model—Formulation. *J. Atmos. Sci.,* **57,** 1741–1766.

Pantoine, A., and T. Warn, 1982: The interaction of long, quasi-stationary waves with topography. *J. Atmos. Sci.,* **39,** 1018–1025.

Wang, B., and X. Xie, 1996: Low-frequency equatorial waves in vertically sheared zonal flow. Part I: Stable waves. *J. Atmos. Sci.,* **53,** 449–467.

Webster, P. J., 1972: Response of the tropical atmosphere to local steady forcing. *Mon. Wea. Rev.,* **100,** 518–541.

——, 1981: Mechanisms determining the atmospheric response to sea surface temperature anomalies. *J. Atmos. Sci.,* **38,** 554–571.

——, 1982: Seasonality in the local and remote atmospheric response to sea surface temperature anomalies. *J. Atmos. Sci.,* **39,** 41–52.